HHS Public Access

Author manuscript

Nat Genet. Author manuscript; available in PMC 2014 August 01.

Published in final edited form as:

Nat Genet. 2014 February ; 46(2): 166–170. doi:10.1038/ng.2873.

Recurrent mutations in epigenetic regulators, *RHOA* and *FYN* kinase in peripheral T cell lymphomas

Teresa Palomero[1,2,17], **Lucile Couronné**[1,17], **Hossein Khiabanian**[3,17], **Mi-Yeon Kim**[1], **Alberto Ambesi-Impiombato**[1], **Arianne Perez-Garcia**[1], **Zachary Carpenter**[3], **Francesco Abate**[3,4], **Maddalena Allegretta**[1], **J. Erika Haydu**[1], **Xiaoyu Jiang**[5], **Izidore S. Lossos**[5,6], **Concha Nicolas**[7], **Milagros Balbin**[8], **Christian Bastard**[9], **Govind Bhagat**[2], **Miguel Angel Piris**[10], **Elias Campo**[11,12], **Olivier Bernard**[13,14,15], **Raul Rabadan**[3], and **Adolfo Ferrando**[1,2,16]

[1]Institute for Cancer Genetics, Columbia University, New York, NY, USA.

[2]Department of Pathology, Columbia University Medical Center, New York, NY, USA.

[3]Joint Centers for Systems Biology, Columbia University, New York, NY, USA.

[4]Department of Control and Computer Engineering, Politecnico di Torino, Torino, Italy

[5]Division of Hematology -Oncology, Sylvester Comprehensive Cancer Center, Miami, FL, USA.

[6]Department of Molecular and Cellular Pharmacology, University of Miami, Miami, FL, USA.

[7]Hematology Service, Hospital Central de Asturias, Oviedo, Spain.

[8]Molecular Oncology Laboratory, Instituto Universitario de Oncologia del Principado de Asturias, Hospital Universitario Central de Asturias, Oviedo, Spain.

[9]INSERM U918 Centre Henri Becquerel, Rouen, France.

[10]Pathology Department, Hospital Universitario Marques de Valdecilla, Santander, Spain.

[11]Hematopathology Section, Department of Pathology, Hospital Clinic, Barcelona, Spain.

[12]Institut d'Investigacions Biomèdiques August Pi i Sunyer, University of Barcelona, Barcelona, Spain.

Correspondence should be addressed to A.F. (af2196@columbia.edu), R.R. (rabadan@dbmi.columbia.edu) and T.P. (tp2151@columbia.edu)..

AUTHOR CONTRIBUTIONS

TP directed and supervised mutation analysis, performed functional assays and wrote the manuscript; LC performed validation and recurrence mutation analysis and functional assays; HK performed exome and RNAseq mutation analysis; MYK performed peptide binding assays; AA analyzed Illumina deep sequencing amplicon sequencing data; APG performed functional assays, ZC performed structure function analysis and analyzed Illumina sequence data; FA performed RNAseq mutation analysis and fusion oncogene identification; MA performed validation analysis of Illumina sequencing results; JEH performed functional assays; XJ performed functional assays; ISL contributed clinical samples and supervised functional assays; CN, MB, CB, GB, MAP and EC contributed clinical samples; OB designed the study, contributed samples and supervised research; RR directed and supervised the analysis of Illumina sequencing data; AF designed the study, directed and supervised research and wrote the manuscript.

Accession codes

Exome data and RNASeq data is available in dbGaP (access code pending).

URLs

Primer 3 is available at http://frodo.wi.mit.edu/primer3/ and BWA-MEM at http://bio-bwa.sourceforge.net

[13]INSERM, U985; Villejuif 94805, France.

[14]Université Paris-Sud, Orsay 91400, France.

[15]Institut Gustave Roussy, Villejuif 94805, France.

[16]Department of Pediatrics, Columbia University Medical Center, New York, NY, USA.

[17]These authors contributed equally to this work

Abstract

Peripheral T-cell lymphomas (PTCLs) are a heterogeneous and poorly understood group of non Hodgkin lymphomas[1,2]. Here we combined whole exome sequencing of 12 tumor-normal DNA pairs, RNAseq analysis and targeted deep sequencing to identify new genetic alterations in PTCL transformation. These analyses identified highly recurrent epigenetic factor mutations in ***TET2, DNMT3A*** **and** ***IDH2*** **as well as a new highly prevalent** ***RHOA*** p.Gly17Val (NM_001664) mutation present in 22/35 (67%) of angioimmunoblastic T-cell lymphomas (AITL) and in 8/44 (18%) not otherwise specified PTCL (PTCL NOS) samples. Mechanistically, the RHOA Gly17Val protein interferes with RHOA signaling in biochemical and cellular assays, an effect potentially mediated by the sequestration of activated Guanine Exchange Factor (GEF) proteins. In addition, we describe new and recurrent, albeit less frequent, genetic defects including mutations in ***FYN, ATM, B2M*** **and** ***CD58*** implicating SRC signaling, impaired DNA damage response and escape from immune surveillance mechanisms in the pathogenesis of PTCL.

To investigate the genetics and pathogenic mechanisms of aggressive PTCLs we performed whole exome sequencing of matched tumor and normal DNA from 12 PTCL patients including 6 PTCL-NOS cases, 3 AITLs and 2 nasal type NK-/T-cell lymphomas and 1 enteropathy associated T-cell lymphoma (**Supplementary Tables 1 and 2**). This analysis identified a mean of 24 non synonymous somatic mutations per sample (range 4 – 57) (**Supplementary Table 1**). A total of 288 candidate coding somatic mutations in 268 genes were identified. These included five mutant alleles in the *TET2* tumor suppressor, three alleles in the *SETD2* and *DNAH5* and two in the *TACC2*, *RYR3*, *PTPRD* and *MGAT4C* genes (**Supplementary Tables 3** and **4**). In addition we identified a recurrent heterozygous mutation in the *RHOA* small GTPase gene (p.Gly17Val) present in two independent AITLs and one PTCL NOS sample (**Fig. 1a** and **Supplementary Tables 3** and **4**). These results were confirmed and extended by deep sequencing analysis of 125 PTCL DNAs, which showed the presence of the recurrent *RHOA* p.Gly17V mutation and detected several additional *RHOA* mutations (p.Cys16Arg, p.Thr19Ile, p.Gly17Glu and p.Asp120Tyr) present in a single case each (**Fig. 1a** and **Supplementary Table 5**). Notably the frequency of the allele encoding the Gly17Val alteration correlated with the proportion of tumor cells in PTCL biopsies as evaluated by multicolor flow cytometry (**Supplementary Figure 1**), supporting that the variable and frequently low proportion of reads harboring this mutation in many PTCLs may be primarily the result of the low tumor content in these samples. Thus, and to best assess the actual prevalence of *RHOA* p.Gly17Val alteration in our series we reanalyzed this panel using a highly sensitive (1:1,000) allele specific PCR mutation assay. Using this approach we detected the presence of the allele encoding the Gly17Val mutant RHOA in 30 samples including 22/35 (67%) AITLs and 8/44 (18%) PTCL NOS tumors

analyzed (AITL *vs.* all other PTCLs: $P < 0.001$; PTCL NOS *vs.* non-AITL non-PTCL NOS: $P < 0.002$; AITL *vs.* PTCLs NOS: $P < 0.001$) (**Fig. 1b,c, Supplementary Figure 2** and **Supplementary Table 6**).

RHOA belongs to the Rho family of small GTPases, a group of Ras-like proteins responsible for linking a variety of cell-surface receptors to different intracellular signaling proteins[3-5]. As is the case for RAS and most other small GTPases, RHOA cycles between inactive – GDP-bound– and active –GTP-bound– configurations[4,5], a molecular switch strictly controlled by the GTP loading activity of guanosine exchange factor proteins (GEFs)[4,5]. In its active configuration, GTP RHOA interacts with multiple downstream effectors that control the structure and dynamics of the actin cytoskeleton and the formation of stress fibers[6]. Given the recurrent nature of the *RHOA* pGly17Val mutation we postulated that this allele could represent a gain of function mutation with either constitutively active or dominant negative activity.

The RHO-family of GTPases, including RHOA, regulates actin cytoskeleton and cell adhesion and is implicated in cell polarization in multiple cell types[6,7]. Thus, in order to explore the functional effects of RHOA Gly17Val we analyzed the changes in fibroblast cell morphology induced by expression of GFP-RHOA wild type, constitutively active GFP-RHOA Gln63Leu[8-11], dominant negative GFP-RHOA Thr19Asn[10-12] and GFP-RHOA Gly17Val fusions. Activation of RHOA signaling triggered by GFP-RHOA overexpression and most prominently by the constitutively active GFP-RHOA Gln63Leu induced loss of adhesion and round cell morphology in HEK293T cells (**Fig. 2a**). In contrast, cells expressing GFP-RHOA Gly17Val mimicked the phenotype of fibroblasts expressing dominant negative GFP-RHOA Thr19Asn, which showed increased elongated morphology and cellular protrusions (**Fig. 2a**). Similarly, immunofluorescence analysis of F-actin in HeLa cells showed increased stress fiber formation in cells expressing GFP-RHOA, which was markedly accentuated upon constitutive activation of RHOA signaling triggered by the GFP-RHOA Gln63Leu mutant (**Fig. 2b**). On the other hand, cells expressing GFP-RHOA Gly17Val or GFP-RHOA Thr19Asn showed decreased F-actin stress fibers, which is consistent with an inhibitory role of these mutations in RHO signaling (**Fig. 2b**).

Following on these results, we expressed HA-tagged forms of wild type RHOA and RHOA Gly17Val in Jurkat T-cells and tested their capacity to interact with rhotekin, an effector protein that specifically recognizes the active GTP-bound form of RHOA[13]. Rhotekin pull down analysis showed significant activation of HA-RHOA in Jurkat cells in basal conditions, which was further increased upon serum stimulation (**Fig. 2c**). In contrast, rhotekin failed to interact with HA-RHOA Gly17Val (**Fig. 2c**). Similarly, rhotekin did not interact with dominant negative HA-RHOA Thr19Asn, while the constitutively active HA-RHOA Gln63Leu protein showed marked increased rhotekin binding (**Fig. 2c**). Given that rhotekin selectively binds to the GTP-bound form of RHOA, we hypothesized that RHOA Gly17Val is locked in an inactive configuration devoid of GTP. Indeed, a highly related RHOA Gly17Ala mutant protein capable of interacting with GEF proteins with high affinity, but resistant to GEF-induced GTP loading and activation has been described [14]. To test this hypothesis, we analyzed the capacity of GSTRHOA, GST-RHOA Gly17Val and GST-RHOA Gly17Ala recombinant proteins to bind to GTP in response to MCF2L/DBS GEF

stimulation *in vitro* using a fluorescence polarization assay. As expected, MCF2L/DBS triggered the loading of a fluorescent GTP analog (mant-GTP) into GST-RHOA (**Fig 2d**). However, GST-RHOA Gly17Ala and GST-RHOA Gly17Val were resistant to the activity of this GEF factor (**Fig. 2d**). Finally, we tested if RHOA Gly17Val could function as a high affinity GEF trap analogous to RHOA Gly17Ala sequestering activated GEF proteins in T-cells. GST pull down assays against ARHGEF1, a GEF factor highly expressed in T-cells, showed increased affinity of GST RHOA Gly17Val and most markedly GST-RHOA Gly17Ala compared to GST-RHOA wild type (**Fig.2e**). Overall, these results are consistent with an inhibitory role for RHOA Gly17Val in RHO signaling potentially mediated by the sequestration of GEF factors and support a role for disruption of RHOA signaling in the pathogenesis of PTCLs.

Next, and to more broadly assess the presence of recurrent genetic alterations and fusion oncogenes in PTCL we analyzed a cohort of 34 lymphoma samples by RNAseq (**Supplementary Table 7**). This analysis identified 4 samples harboring *ALK* fusion transcripts (3 *NPM-ALK* and 1 *TFG-ALK*), all corresponding to ALCL cases (**Supplementary Table 8**). In addition we detected the presence of candidate recurrent mutations in *TET2*, *DNMT3A* and *IDH2* and identified additional potential drivers of PTCL transformation (**Supplementary Table 9**). Deep sequencing analysis of these and additional selected candidate genes including FYN, TET3, CDKN2A, PRKD2, RHOT2, SMARCAL1, ATM, B2M and *CD58* in an extended panel of 125 PTCL DNAs including those analyzed by RNAseq showed a prominent role of mutations targeting DNA methylation and hydroxymethylation (*TET2*, *DNMT3A*, *IDH2* and *TET3*) as shown before[15-17] and highlighted the role of defective DNA damage response (*ATM*) and escape from T-cell and NK cell immune surveillance (*B2M* and *CD58*) in the pathogenesis of PTCL (**Fig. 3b** and **Supplementary Table 5**). In addition, we detected the presence of new recurrent *FYN* kinase (NM_002037) mutations including a recurrent allele encoding a p.Arg176Cys substitution present in two PTCL NOS cases, a mutation encoding a p.Leu174Arg alteration found in one AITL patient sample, in addition to the p.Tyr531His encoding allele identified via exome analysis in a PTCL NOS sample for an overall frequency of 3% (4/137) *FYN* mutations in our series (**Fig. 3b** and **Supplementary Table 5**).

The FYN tyrosine kinase is, with LCK, the predominant SRC family kinase found in T lymphocytes and plays an important role in T-cell activation upon T-cell receptor (TCR) stimulation[18]. Strikingly, *FYN* mutations found in PTCL are predicted to specifically disrupt the intramolecular inhibitory interaction of the FYN SH2 domain with C-terminal SRC kinase (CSK) phosphorylated FYN Tyr531. Consistently, expression of FYN Leu174Arg, FYN Arg176Cys and FYN Tyr531His in Rat1A cells resulted in increased levels of FYN activation compared with control cells expressing wild type FYN (**Fig. 4a,b**). In addition, structure model analysis of FYN and FYN mutant proteins further supported this hypothesis (**Fig. 4c,d**). To test this model, we analyzed the interaction between GST-FYN-SH2 recombinant proteins and biotinylated C-terminal FYN peptides encompassing the position Tyr531. In these assays, wild type GST-FYNSH2 was effectively pulled down with a Tyr531 phosphopeptide, but not with the corresponding unphosphorylated sequence or with a peptide containing a Tyr531His substitution (**Fig. 4e**). Similarly, the introduction of a

Leu174Arg or a Arg176Cys substitution abrogated the interaction of GST-FYN-SH2 with the phospho-Y531 FYN C-terminal peptide (**Fig. 4f**). Consistently, CSK effectively inhibited wild type FYN, but failed to abrogate the activity of the FYN mutant proteins (**Fig. 4g**). Finally, given the prominent role of kinase inhibitors as targeted therapies for tumors driven by constitutively active kinase oncogenes, we tested the capacity of dasatinib, a multikinase inhibitor which blocks ABL1 and SRC kinases[19], to inhibit the activity of FYN Leu174Arg, FYN Arg176Cys and FYN Tyr531His mutant proteins. Notably, in each case, dasatinib treatment induced dose dependent inhibition of FYN phosphorylation (**Fig. 4h**). Moreover, dasatinib treatment impaired the growth of transformed Rat1A cells expressing the FYN Tyr531His mutant protein, but not that of cells expressing a drug-resistant gatekeeper mutant form of this kinase (FYN Thr342Ile Tyr531His) (**Fig. 4i,j**). Based on these results we propose that SRC kinase inhibition with dasatinib may confer a therapeutic benefit in selected PTCL cases harboring activating mutations in the *FYN* kinase gene.

METHODS

Patient samples

DNAs from PTCLs were provided by tumor banks at Columbia University Medical Center in New York, USA; Sylvester Comprehensive Cancer Center, Miami, USA; Hospital Central de Asturias in Oviedo, Spain; Centro Nacional de Investigaciones Oncologicas in Madrid, Spain; Institut Gustave Roussy, Villejuif, France; Centre Henri Becquerel, Rouen, France; and Hospital Clinic in Barcelona, Spain. Samples were obtained with informed consent and analysis was conducted under the supervision of the Columbia University Medical Center Institutional Review Board. We selected samples for Whole Exome Sequencing based on the availability of sufficient DNA from diagnosis, and normal (blood, buccal swab or non tumor infiltrated biopsy material) matched samples.

Whole exome capture and nextgen sequence analysis

We used matched tumor and normal DNA samples from 12 PTCL patients (**Supplementary Table 1**) for exome capture with the SureSelect 50 Mb All Exon kit (Agilent Technologies) following standard protocols. We performed paired-end sequencing (2 × 100 bp) using HiSeq2000 sequencing instruments at Centrillion Biosciences (Palo Alto, CA). Illumina HiSeq analysis produced between 67.5 and 136.8 million paired-end reads per sample (**Supplementary Table 2**). We mapped reads to the reference genome hg19 using the Burrows-Wheeler Aligner (BWA) alignment tool version 0.5.9. Mean depth (defined as mean number of reads covering the captured coding sequence of a haploid reference) was 45x with 84% of the genome covered more than 10× and 58% covered more than 30×. We identified sites that differ from reference (called here variants) in each sample independently. We constructed empirical priors for the distribution of variant frequencies for each sample. We obtained high-credibility intervals (posterior probability ≥ $1–10^{-5}$) for the corresponding change in frequency between tumor and normal samples, using the SAVI algorithm (Statistical Algorithm for Variant Identification) developed at Columbia University[32,33]. The number of germline SNPs in the coding region were 18,000 comparable with previous reports[32]. Most of the candidate germline SNPs (16,000, or ~90% of germline variants) were reported in dbSNP database. We identified candidate somatic variants using

the following criteria: variant total depth in tumor and normal larger than 10× and smaller than 300×, variant frequency larger than 15% in tumor and less than 3% in normal, and at least 1% change in frequency from the normal with high posterior probability ($\geq 1–10^{-5}$). Also to remove systematic errors, we excluded all variants that were found present in any of the normal cases. In addition, to eliminate ambiguous mapping from captured pseudogenes, and regions of low complexity, each variant with a flanking 20-base context sequence around its genomic position was mapped to the hg19 reference using the BLAST algorithm. We kept in the list only those with unique mappability, i.e. we required the 41-base sequence to uniquely map to the reference genome, with only one mismatch.

Mutation validation

We designed primers flanking exons containing 121 randomly selected candidate somatic variants identified by exome sequencing using Primer3, and used Whole-Genome-Amplified (WGA) DNA from tumor and matched normal DNAs for PCR amplification. We analyzed the resulting amplicons by direct bidirectional dideoxynucleotide sequencing and obtained a validation rate of 90% (**Supplementary Table 1**).

RNA Sequencing, mapping, and identification of variants

After the exome sequence analysis of 12 tumor and normal PTCL samples (**Supplementary Table 1**); we analyzed 34 additional PTCL samples by RNA-Seq using paired-end Illumina Hiseq sequencing. (**Supplementary Table 7**). We obtained on average over 67.6 million reads, 51.5 million (75.7%) mapped to the human NCBI reference sequence (RefSeq) using BWA alignment algorithms[20]. Reads mapping on the same starting position were discarded. We identified sites that differed from the reference in each sample and constructed empirical priors for the distribution of variant frequencies for each sample independently. In order to reduce the false positive rate in variants detection and remove mapping artifacts and systematic errors, we mapped samples' paired-end reads to human RefSeq with Bowtie2 alignment algorithm[21], which mapped a total of 1.83 billion reads of reads (76%) properly to the reference. We then identified sites that differed from the reference in each sample and intersected the set of variants identified with both BWA and Bowtie2 alignments as previously described[22]. In all samples, we selected variants with total depth >10× and frequency >20%, and excluded variants identified in dbSNP135 database, as well as those which did not pass the Multiplicity filter. In addition, variants corresponding to poorly expressed (RPKM < 3) genes were removed to reduce the effects of spurious PCR amplification during library preparation. In order to reduce the presence of germline mutations, variants identified also present in 65 DNA-Seq samples from unaffected individuals were excluded and we removed also variants common to those present in 11 RNASeq samples from normal B and T cells. In detail, we mapped the normal RNA-Seq sample reads with BWA and Bowtie to human RefSeq and identified the variants, creating an internal normal variant database (INVD) composed by the union of all the variants identified in normal B and T cells. Successively, we filtered those variants occurring in PTCL samples overlapping the INVD. Finally, we limited the list of variants to those identified in genes found somatically mutated in PTCL by exome sequencing.

Targeted deep resequencing

Mutational analysis of selected genes of interest was performed by targeted resequencing using microfluidics PCR (Access Array system; Fluidigm) followed by sequencing of the amplicon libraries in a MiSeq instrument (Illumina). Primers targeting the regions of interest were designed at Fluidigm to produce amplicons of 200 bp ± 20 bp. We performed multiplex PCR amplification of up to 10 amplicons per well in the Fluidigm Access Array chip according to the manufacturer's instructions using 30 ng of DNA per sample. After multiplex PCR amplification the resulting DNA products were barcoded so that all amplicons corresponding to the one sample carry the same index. Indexed libraries were pooled and the resulting library was quantified by quantitative PCR using the Kapa Library Quantification Kit (Kapa Biosystems) in a 7500 PCR instrument (Applied Biosystems). Amplicon libraries were spiked with ~25% PhiX genomic library to increase amplicon diversity and sequenced in a MiSeq instrument to generate 2×251 bp paired reads following an amplicon sequencing protocol for custom primers. Each pair of the paired end reads produced by MiSeq were stitched together using FLASH version 1.2.6 (Fast Length Adjustment of SHort reads), given that the amplicon sequences (up to 200 bp) were shorter than the read length (251 bp). This step increases the quality of the reads correcting for mismatches in the overlap by selecting the base with higher quality. Then, 5' and 3' adaptors and PCR primer sequences, were trimmed using cutadapt. Merged and trimmed reads were aligned to the UCSC hg19 reference genome using BWA-MEM as single-end reads. Aligned reads were analyzed for variants using the SAVI (Statistical Algorithm for Variant Identification) algorithm and variants were selected based on coverage depth and frequency. Given the presence of significant normal cells in most PTCL samples, variants around 50% frequency were flagged as candidate private germline SNPs. Candidate variants identified by this first round of amplicon resequencing were independently validated in a second round of targeted deep sequencing. Briefly, we selectively amplified the amplicons covering the positions of candidate mutations in their corresponding positive samples, barcoded these PCR products, pooled them and sequenced the resulting library in a MiSeq instrument as detailed before.

RNAseq gene fusion analysis

We performed gene fusion analysis in RNAseq data using ChimeraScan [23] and deFuse [24] algorithms, which identify gene fusion candidates by detecting read pairs discordantly mapping to two different genes. From this analysis we then successively reduced the candidate list by applying homology-based filters and by detecting reads spanning across the junction breakpoint (Split Reads). Finally, we annotated candidate fusions on the base of the breakpoint coordinates, predicted amino acid sequence, open reading frame conservation and UniProt database proteomic information.

Quantitative *RHOA* p.Gly17Val allele specific qPCR assay

Analysis and quantitation of *RHOA* p.Gly17Val was performed using a Mutation Detection Assay Competitive Allele-Specific TaqMan® PCR (Life Technologies) following the manufacturer's instructions with slight modifications. All analyses were conducted on a 7500 real-time PCR system run with 7500 software (v.2.0.6 Applied Biosystems). The assay

was run in 96-well plates in a reaction volume of 20 μL, using 50 ng of genomic DNA, 10 μL of Taqman Universal PCR Master Mix 2x, and 2 μL of specific Taqman assay 10× (*RHOA* wild type or *RHOA* p.Gly17Val). We used a thermal profile of 10 min at 95°C for Hot Gold Start activation followed by 40 cycles of amplification (95°C for 15 s and 55°C for 60 s). The threshold detection was set at 0.05. Standard curves of C_T *vs.* log template amount for each specific assay were linear over the range of 25 to 250,000 copies of plasmid DNA. We determined a sensitivity of detection for the *RHOA* p.Gly17Val mutant allele assay of <0.1% by analyzing samples consisting of 10, 25, 10^2 and 10^3 copies of *RHOA* p.Gly17Val mutant allele plasmid DNA spiked into 30 ng (10^4 copies) of wild type genomic DNA, which corresponds to samples containing 0.1%, 0.25%, 1% or 10% mutation load, respectively. Data analysis was performed with the Mutation Detector™ Software (Life Technologies). Briefly, in mutation analysis calculations, the difference between the C_T value of the mutant allele assay and the C_T value of the wild type allele assay is calculated for all mutant allele assays run on the sample. This ΔC_T value represents the quantity of the specific mutant allele detected within the sample and is used to determine the sample mutation status by comparison to a predetermined detection ΔC_T cutoff value.

Structural depiction and analysis

We identified structural coverage of the FYN protein through use of the PSI-Blast and SKAN algorithms. The structures 2DQ7, 2DLY, 3UA7, 2LP5, and 1G83 were structurally aligned into composite structures to assess for conformational flexibilities, and subsequently analyzed through use of the Chimera Suite[25,26]. In silico modeling of identified mutations was performed using the I-TASSER software suite and Modeller program; structures were refined and analyzed in Chimera[25,27]. We predicted protein stability changes upon mutation through use of the SDM potential energy statistical algorithm and associated software[37]. We created all structural images using UCSF Chimera[25].

Plasmids and vectors

We obtained pcDNA3 EGFP-RHOA WT (plasmid#12965) containing the full length human RHOA construct fused to EGFP as well as pcDNA3 EGFP-RHOA Thr19Asn dominant negative (plasmid #12967) and pcDNA3 EGFP-RHOA Gln63Leu constitutively active mutants (plasmid #12968) from Addgene, Inc[28]. We generated the *RHOA* p.Gly17Val allele by site directed mutagenesis on the mammalian expression pcDNA3 EGFPRHOA WT using the QuickChange II XL Site-Directed Mutagenesis Kit (Stratagene) according to the manufacturer's instructions. We cloned PCR products encompassing wild type *RHOA*, *RHOA* p.Gly17Val, *RHOA* p.Thr19Asn and *RHOA* p.Gln63Leu with an N-terminal HA tag as *BglII-XhoI* fragments into the pMSCV vector for retroviral expression. We obtained pRK5 c-FYN plasmid containing a full length *FYN* open reading frame[29] from Addgene, Inc. (Plasmid #16032) and introduced *FYN* p.Leu174Arg, *FYN* p.Arg176Cys, *FYN* p.Tyr531His and *FYN* p.Thr342Ile Tyr531His mutations using the QuickChange II XL Site-Directed Mutagenesis Kit (Stratagene). All constructs were verified by sequencing. Wild type and mutant FYN cDNAs containing an N-terminal HA tag were subcloned into pcDNA3.1(–) and into the MSCV240-puromycine-IRES-GFP retroviral vector. The CSK-pcDNA3.1 (+) hygro plasmid expressing a full length CSK cDNA open reading frame was a gift from Dr. Xin-Yun Huang (Cornell University, New York, NY). We cloned FYN SH2

domain complementary DNA constructs encoding wild type FYN SH2 domain (codons 148-231) with an N-terminal GST tag in the pGEX4-T1 expression vector between the *EcoRI* and *XhoI* restriction sites. We generated the FYN SH2 domain mutations Leu174Arg and Arg176Cys by site-directed mutagenesis on the *E. coli* expression pGEX4-T1 FYN SH2 domain vector using the QuikChange II XL Site-Directed Mutagenesis Kit (Stratagene) according to the manufacturer's instructions.

Cell lines

We cultured HEK293T (Thermo Scientific), HeLa (ATCC) and Rat1A cells (a gift from Dr. Ana Lasorella, Columbia University) in DMEM media supplemented with 10% fetal bovine serum, 100 U ml^{-1} penicillin G and 100 μg ml^{-1} streptomycin at 37°C in a humidified atmosphere under 5% CO_2. We maintained Jurkat cells (ATCC) under similar conditions in RPMI 1640 media supplemented with 10% fetal bovine serum. Cell lines were regularly tested for mycoplasma contamination.

Retroviral production and infection

We transfected the retroviral constructs pMSCV-HARHOA, pMSCV-HA-RHOA Gly17Val, pMSCV-HA-RHOA Gln63Leu, pMSCV-HA-RHOA Thr19Asn, pMSCV-FYN, pMSCV-FYN Tyr531His, pMSCV-FYN Thr342Ile Tyr531His, pMSCVFYN Arg176Cys, pMSCV-FYN Leu174Arg and the pMSCV control plasmid with gag-pol and VSVG expressing vectors into HEK293T cells using JetPEI transfection reagent (Polyplus). We collected viral supernatants after 48h and used them for infection of Rat1A and Jurkat cells by spinoculation. After infection, we selected cells for 4 days in media containing 1 μg/ml of puromycin.

Western blot

Western blot analysis were performed using standard procedures with the following antibodies: RHOA (67B9) rabbit monoclonal antibody against RHOA (#2117, Cell Signaling Technology)[30]; FYN rabbit polyclonal antibody (#4023, Cell Signaling Technology)[31]; Phospho-Src Family (Tyr416) polyclonal antibody (#2101, Cell Signaling Technology)[32]; CSK (CSK-04) mouse monoclonal antibody (sc-51580, Santa Cruz Biotechnology); GST mouse monoclonal antibody (clone DG122-2A7, Millipore, 1DB-001-0000851588)[33]; GAPDH goat polyclonal antibody (sc-20357, Santa Cruz Biotechnology)[34]; ARGHEF1 goat polyclonal antibody (sc-8492, Santa Cruz Biotechnology)[35] and a rat monoclonal antibody specific for HA tag (11867423001, Roche Diagnostics, 1DB-001-0000868977).

Immunofluorescence

We analyzed F-actin in Hela cells transfected with plasmids expressing GFP, GFP-RHOA, GFP-RHOA Gln63Leu, GFP-RHOA Thr19Asn and GFP-RHOA Gly17Val by Phalloidin Texas Red staining (1:100; Life Technologies), followed by DAPI (4',6-Diamidino-2-Phenylindole, Dihydrochloride) staining and confocal microscopy on a Zeiss LSM510-NLO microscope.

RHOA protein expression in *Escherichia coli*, purification, and GEF exchange assay

We expressed wild type RHOA, RHOA Gly17Ala and RHOA Gly17Val proteins as GST-tagged proteins in *E. coli* Rosetta 2(DE3) cells. We induced expression of the fusion proteins in bacteria cells with 0.1 mM isopropyl-β-D-thiogalactopyranoside (IPTG) for 16h at 18°C. We harvested cells and lysed them in lysis buffer (20 mM Hepes, pH 7.5, 150 mM NaCl, 5mM MgCl2, 1 mM DTT, 1% Triton X-100, 0.5 mg / ml lysozyme) supplemented with Complete EDTA-free protease inhibitor (Roche). We purified GST-tagged RHOA proteins by binding them to immobilized glutathione Sepharose beads (Thermo scientific) and eluting them with 50 mM reduced Glutathione, 50 mM HEPES, pH 7.4, 150 mM NaCl, 5 mM $MgCl_2$, 5 % glycerol, 1 mM DTT. We assessed protein expression and purity by Coomassie staining. Next, we analyzed the capacity of purified recombinant GST-RHOA, GST-RHOA Gly17Ala and GST-RHOA Gly17Val proteins to incorporate GTP in response to recombinant MCF2L/DBS-His (Cytoskeleton, Inc.) with the RhoGEF exchange assay kit (Cytoskeleton, Inc.) following the manufacturer's instructions. Briefly, this assay analyzes the uptake of the fluorescent nucleotide analog N-methylanthraniloyl-GTP (mant-GTP) into RHOA by measuring the spectroscopic difference between free and RHOA-bound mant-GTP. As mant-GTP gets bound in the nucleotide binding pocket of RHOA in response to a GEF protein, its fluorescence (ex: 360 nm, em: 440 nm) increases dramatically. Thus, enhancement of mant-GTP fluorescent intensity in the presence of RHOA indicates nucleotide uptake by the GTPase.

RHOA activation assay

We used Jurkat cells expressing wild type HA–RHOA, HA-RHOA Gly17Val, HA-RHOA Thr19Asn and HA-RHOA Gln63Leu and plated them at 10^6 cells/ml in RPMI 0.5% FBS. After 24 hours we spun them down and resuspended in serum-free RPMI 1640 media. For serum stimulation cells were treated with media containing 10% FBS for 10 min. We washed serum starved and serum stimulated cells once with ice cold PBS and lysed them in Lysis buffer (50 mM Tris pH 7.5, 10 mM $MgCl_2$, 0.3 M NaCl and 2% IGEPAL). After spinning down to remove debris and membranes we quantified lysate protein content using the Precision Red Advanced Protein Assay (Cytoskeleton, Inc.). Next we incubated 100 μg of total cleared protein lysate with 20 μl Rhotekin-RBD beads (Cystoskeleton, Inc.) for 1h at 4°C with rotation. After incubation we washed the Rhotekin-RBD beads with 500 μl wash buffer (25 mM Tris pH 7.5, 30 mM $MgCl_2$ and 40 mM NaCl), resuspended them in 15 μl SDS-PAGE loading buffer. Rhotekin bead samples were loaded into a Bis-Tris gel and proteins were resolved by electrophoresis in MES buffer and transferred to a PVDF membrane. The presence of HA-tagged activated RHOA associated with the Rhotekin-RBD beads was determined by immunoblotting using an HA antibody following standard procedures.

Immunoprecipitation and Western blot analysis of FYN activation

We performed FYN immunoprecipitations in Rat1A cells infected with control (empty vector) retroviruses or retroviruses expressing wild type FYN, FYN Leu174Arg, FYN Arg176Cys and FYN Tyr531His and analyzed FYN phosphorylation via Western blot

analysis using a Phospho-Src Family (Tyr416) polyclonal antibody (#2101, Cell Signaling Technology).

FYN protein expression in *Escherichia coli*, purification, and peptide binding assays

We expressed wild type and mutant FYN SH2 domain as GST-tagged proteins in *E. coli* Rosetta 2(DE3) cells as detailed for the production of GST-RHOA fusion proteins before. Next, we performed peptide binding assays with Pull-Down Biotinylated Protein-protein Interaction Kit (Thermo scientific) according to the manufacturer's instructions using an amino acid 527-537 FYN biotinylated peptide (biotin-Thr Glu Pro Gln Tyr Gln Pro Gly Glu Asn Leu); an amino acid 527-537 pTyr531 FYN biotinylated peptide (biotin- Thr Glu Pro Gln pTyr Gln Pro Gly Glu Asn Leu) and an amino acid 527-537 Tyr51His FYN biotinylated peptide (biotin- Thr Glu Pro Gln His Gln Pro Gly Glu Asn Leu) (Anaspec Inc). Briefly, we incubated synthetic biotinylated peptides with purified GST-FYN SH2 domain, mutant FYN SH2 domain or GST alone proteins for 1 h at 4°C, resolved and analyzed interacting proteins via 10% SDS-polyacrylamide gel electrophoresis (SDS-PAGE) followed by transfer to a PVDF membrane and Western blot analysis with an anti-GST antibody.

CSK FYN inhibition assay

We transfected Hela cells with plasmids driving expression of wild type (pRK5 c-FYN) and activating mutant FYN alleles (pRK5 FYN Leu174Arg, pRK5 FYN Arg176Cys and pRK5 FYN Tyr531His) alone and with a vector driving expression of CSK (CSK-pcDNA3.1) at ratios 1:1 and 1:3 and analyzed the levels of FYN activation and FYN and CSK expression via Western blot analysis.

Dasatinib FYN inhibition assays

We transfected HEK293T cells with vectors driving the expression of activated mutant FYN proteins (pRK5 FYN Leu174Arg, pRK5 FYN Arg176Cys and pRK5 FYN Tyr531His). After 48 hours cell cultures were treated with increasing concentrations of dasatinib (Selleck Chemicals) for 6 hours and analyzed for FYN phosphorylation and FYN expression by Western blot analysis. Similarly, transformed Rat1A cells expressing the FYN Tyr531His mutant or a double FYN Thr342Ile Tyr531His mutant protein were treated with vehicle only or dasatinib (1μM) for 6 hours and analyzed for FYN phosphorylation and FYN expression by Western blot analysis.

Cell proliferation assays

We analyzed relative cell growth at 72 hours of vehicle only treated and dasatinib treated (1μM) Rat1A transformed cells expressing either the FYN Tyr531His mutant or a double FYN Thr342Ile Tyr531His mutant protein. Cell growth was determined in triplicates by measurement of the metabolic reduction of the tetrazolium salt MTT using the Cell Proliferation Kit I (Roche) following the manufacturer's instructions.

Statistical analyses

We evaluated differences in the percentages of *RHOA* wild type and *RHOA* Gly17Val mutant in different PTCL groups using the Fisher's exact test. We analyzed differences in

cell growth rates in control and dasatinib treated cells using the Student's *t* test. We tested the linear correlation between tumor content in PTCL samples and *RHOA* p.Gly17Val allele burden with the coefficient of determination R^2.

Supplementary Material

Refer to Web version on PubMed Central for supplementary material.

ACKNOWLEDGEMENTS

This work was supported by a Leukemia & Lymphoma Society Translational Research Grant (A.F.), a Herbert Irving Comprehensive Cancer Center interprogrammatic pilot project grant (A.F. & R.R.), a National Institutes of Health Ruth L. Kirschstein National Research Service Award (1F30CA174099 to J.E.H.), a grant from the Ligue Nationale Contre le Cancer (O.B.) and an INCa-DHOS translational research grant (O.B.). L.C. is a postdoctoral researcher funded by ITMO (Institut Multi Organismes Cancer, France) and INCa (Institut National du Cancer, France). M.Y.K. is a postdoctoral researcher funded by the Leukemia and Lymphoma Society. We would like to thank Dr. Vincent Ribrag (Institut Gustave Roussy, Villejuif, France) for providing a PTCL sample and Dr. Ramon Parsons (Mount Sinai School of Medicine, New York, USA) for assistance in the set up of RHOA GTP loading assays.

REFERENCES

1. Armitage JO. The aggressive peripheral T-cell lymphomas: 2012 update on diagnosis, risk stratification, and management. Am J Hematol. 2012; 87:511–9. [PubMed: 22508369]
2. Rudiger T, et al. Peripheral T-cell lymphoma (excluding anaplastic large-cell lymphoma): results from the Non-Hodgkin's Lymphoma Classification Project. Ann Oncol. 2002; 13:140–9. [PubMed: 11863096]
3. Schiller MR. Coupling receptor tyrosine kinases to Rho GTPases--GEFs what's the link. Cell Signal. 2006; 18:1834–43. [PubMed: 16725310]
4. Bar-Sagi D, Hall A. Ras and Rho GTPases: a family reunion. Cell. 2000; 103:227–38. [PubMed: 11057896]
5. Vega FM, Ridley AJ. Rho GTPases in cancer cell biology. FEBS Lett. 2008; 582:2093–101. [PubMed: 18460342]
6. Hanna S, El-Sibai M. Signaling networks of Rho GTPases in cell motility. Cell Signal. 2013
7. Hall A. Rho family GTPases. Biochem Soc Trans. 2012; 40:1378–82. [PubMed: 23176484]
8. Longenecker K, et al. Structure of a constitutively activated RhoA mutant (Q63L) at 1.55 A resolution. Acta Crystallogr D Biol Crystallogr. 2003; 59:876–80. [PubMed: 12777804]
9. Mayer T, Meyer M, Janning A, Schiedel AC, Barnekow A. A mutant form of the rho protein can restore stress fibers and adhesion plaques in v-src transformed fibroblasts. Oncogene. 1999; 18:2117–28. [PubMed: 10321736]
10. Zhang S, et al. Rho family GTPases regulate p38 mitogen-activated protein kinase through the downstream mediator Pak1. J Biol Chem. 1995; 270:23934–6. [PubMed: 7592586]
11. Ghosh PM, et al. Role of RhoA activation in the growth and morphology of a murine prostate tumor cell line. Oncogene. 1999; 18:4120–30. [PubMed: 10435593]
12. Pan ZK, et al. Role of the Rho GTPase in bradykinin-stimulated nuclear factor-kappaB activation and IL-1beta gene expression in cultured human epithelial cells. J Immunol. 1998; 160:3038–45. [PubMed: 9510209]
13. Reid T, et al. Rhotekin, a new putative target for Rho bearing homology to a serine/threonine kinase, PKN, and rhophilin in the rho-binding domain. J Biol Chem. 1996; 271:13556–60. [PubMed: 8662891]
14. Garcia-Mata R, et al. Analysis of activated GAPs and GEFs in cell lysates. Methods Enzymol. 2006; 406:425–37. [PubMed: 16472675]
15. Couronne L, Bastard C, Bernard OA. TET2 and DNMT3A mutations in human T-cell lymphoma. N Engl J Med. 2012; 366:95–6. [PubMed: 22216861]

16. Quivoron C, et al. TET2 inactivation results in pleiotropic hematopoietic abnormalities in mouse and is a recurrent event during human lymphomagenesis. Cancer Cell. 2011; 20:25–38. [PubMed: 21723201]
17. Cairns RA, et al. IDH2 mutations are frequent in angioimmunoblastic T-cell lymphoma. Blood. 2012; 119:1901–3. [PubMed: 22215888]
18. Palacios EH, Weiss A. Function of the Src-family kinases, Lck and Fyn, in T-cell development and activation. Oncogene. 2004; 23:7990–8000. [PubMed: 15489916]
19. McCormack PL, Keam SJ. Dasatinib: a review of its use in the treatment of chronic myeloid leukaemia and Philadelphia chromosome-positive acute lymphoblastic leukaemia. Drugs. 2011; 71:1771–95. [PubMed: 21902298]
20. Li H, Durbin R. Fast and accurate long-read alignment with Burrows-Wheeler transform. Bioinformatics. 2010; 26:589–95. [PubMed: 20080505]
21. Langmead B, Salzberg SL. Fast gapped-read alignment with Bowtie 2. Nat Methods. 2012; 9:357–9. [PubMed: 22388286]
22. Schmitz R, et al. Burkitt lymphoma pathogenesis and therapeutic targets from structural and functional genomics. Nature. 2012; 490:116–20. [PubMed: 22885699]
23. Maher CA, et al. Chimeric transcript discovery by paired-end transcriptome sequencing. Proc Natl Acad Sci U S A. 2009; 106:12353–8. [PubMed: 19592507]
24. McPherson A, et al. deFuse: an algorithm for gene fusion discovery in tumor RNA-Seq data. PLoS Comput Biol. 2011; 7:e1001138. [PubMed: 21625565]
25. Pettersen EF, et al. UCSF Chimera--a visualization system for exploratory research and analysis. J Comput Chem. 2004; 25:1605–12. [PubMed: 15264254]
26. Altschul SF, et al. Gapped BLAST and PSI-BLAST: a new generation of protein database search programs. Nucleic Acids Res. 1997; 25:3389–402. [PubMed: 9254694]
27. Roy A, Kucukural A, Zhang Y. I-TASSER: a unified platform for automated protein structure and function prediction. Nat Protoc. 2010; 5:725–38. [PubMed: 20360767]
28. Subauste MC, et al. Rho family proteins modulate rapid apoptosis induced by cytotoxic T lymphocytes and Fas. J Biol Chem. 2000; 275:9725–33. [PubMed: 10734125]
29. Mariotti A, et al. EGF-R signaling through Fyn kinase disrupts the function of integrin alpha6beta4 at hemidesmosomes: role in epithelial cell migration and carcinoma invasion. J Cell Biol. 2001; 155:447–58. [PubMed: 11684709]
30. Kamanova J, et al. Adenylate cyclase toxin subverts phagocyte function by RhoA inhibition and unproductive ruffling. J Immunol. 2008; 181:5587–97. [PubMed: 18832717]
31. Pallotta MT, et al. Indoleamine 2,3-dioxygenase is a signaling protein in long-term tolerance by dendritic cells. Nat Immunol. 2011; 12:870–8. [PubMed: 21804557]
32. Harr MW, et al. Inhibition of Lck enhances glucocorticoid sensitivity and apoptosis in lymphoid cell lines and in chronic lymphocytic leukemia. Cell Death Differ. 2010; 17:1381–91. [PubMed: 20300113]
33. Widmann C, Gerwins P, Johnson NL, Jarpe MB, Johnson GL. MEK kinase 1, a substrate for DEVD-directed caspases, is involved in genotoxin-induced apoptosis. Mol Cell Biol. 1998; 18:2416–29. [PubMed: 9528810]
34. Schenk S, et al. Sirt1 enhances skeletal muscle insulin sensitivity in mice during caloric restriction. J Clin Invest. 2011; 121:4281–8. [PubMed: 21985785]
35. Wang Q, et al. Thrombin and lysophosphatidic acid receptors utilize distinct rhoGEFs in prostate cancer cells. J Biol Chem. 2004; 279:28831–4. [PubMed: 15143072]

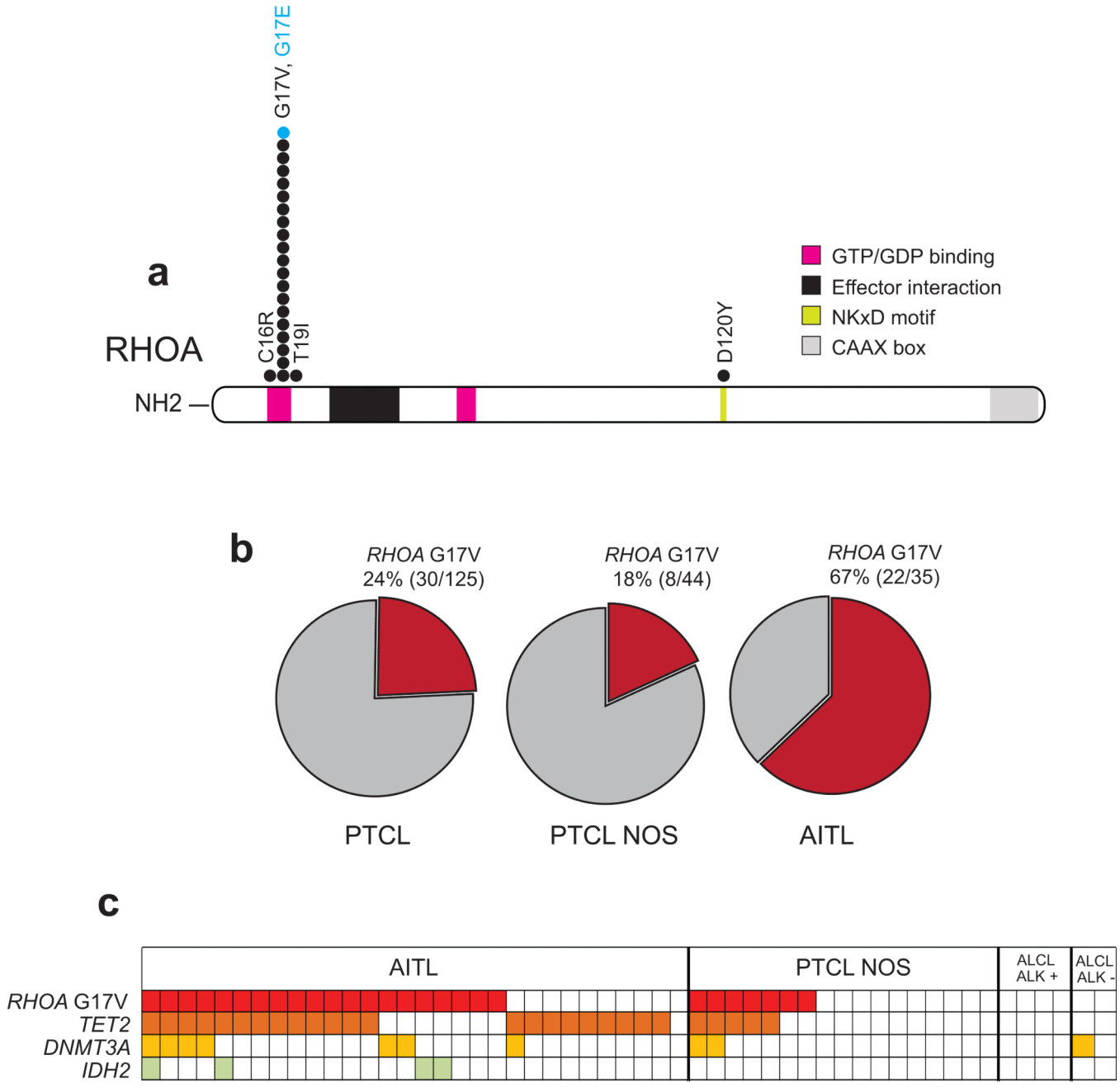

Figure 1. *RHOA* mutations in PTCLs

(**a**) Schematic representation of the structure of the RHOA protein. *RHOA* mutations identified by targeted amplicon resequencing in PTCL samples are shown (n=64). Multiple circles in the same amino acid position account for multiple patients with the same variant. (**b**) Differential distribution of *RHOA* mutations in all PTCL categories, PTCL NOS and AITLs. (**c**) Distribution of *RHOA* p.Gly17Val, *TET2*, *DNMT3A* and *IDH2* mutations in major PTCL groups (AITL, n=30; PTCL NOS, n=17; ALCL ALK+, n=4; and ALCL ALKL–, n=2). Colored boxes indicate the presence of mutations in the indicated genes (rows) in each patient sample (columns).

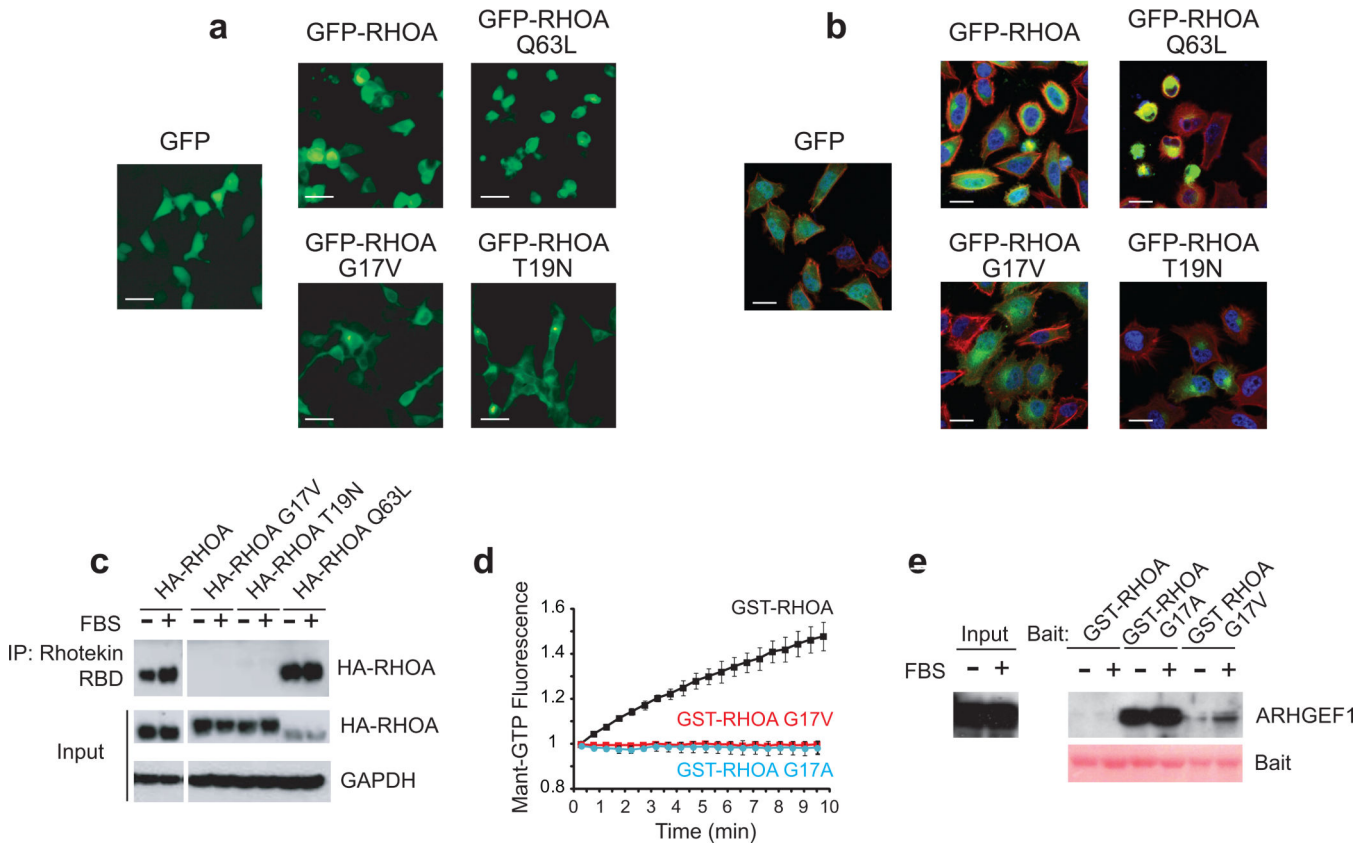

Figure 2. Functional characterization of the RHOA Gly17Val protein

(**a**) GFP fluorescence micrographs of HEK293T cells expressing GFP, GFP-RHOA, constitutively active GFP-RHOA Q63L, dominant negative GFP-RHOA Thr19Asn and GFP-RHOA Gly17Val protein. Scale bar = 10μm. (**b**) Immunofluorescence analysis of stress fiber formation in HeLa cells expressing GFP, GFP-RHOA, GFP-RHOA Gln63Leu, GFP-RHOA Thr19Asn and GFP-RHOA Gly17Val protein shown in green. Actin fibers stained with phalloidin are shown in red and cell nuclei stained with DAPI are shown in blue. Scale bar = 20μm. (**c**) Western blot analysis of GTP-bound HA-RHOA in rhotekin pull downs from Jurkat cells expressing wild type HA-RHOA, constitutively active HARHOA Gln63Leu, dominant negative HA-RHOA Thr19Asn and the PTCL associated HA-RHOA Gly17Val protein. (**d**) Fluorescence polarization analysis of mant-GTP loading to GST-RHOA, GST-RHOA Gly17Ala and GST-RHOA Gly17Val in response to MCF2L/DBS stimulation. (**c**) Western blot analysis of ARHGEF1 GEF protein pulled down with GST-RHOA, GST-RHOA Gly17Ala and GST-RHOA Gly17Val from Jurkat cell lysates in basal conditions and upon serum (FBS) stimulation. Pounceau S staining of bait protein loading is shown at the bottom. Representative images from at least two independent experiments are shown in (**a**) and (**b**). Data in (**d**) shows average ± s.d. from triplicate samples.

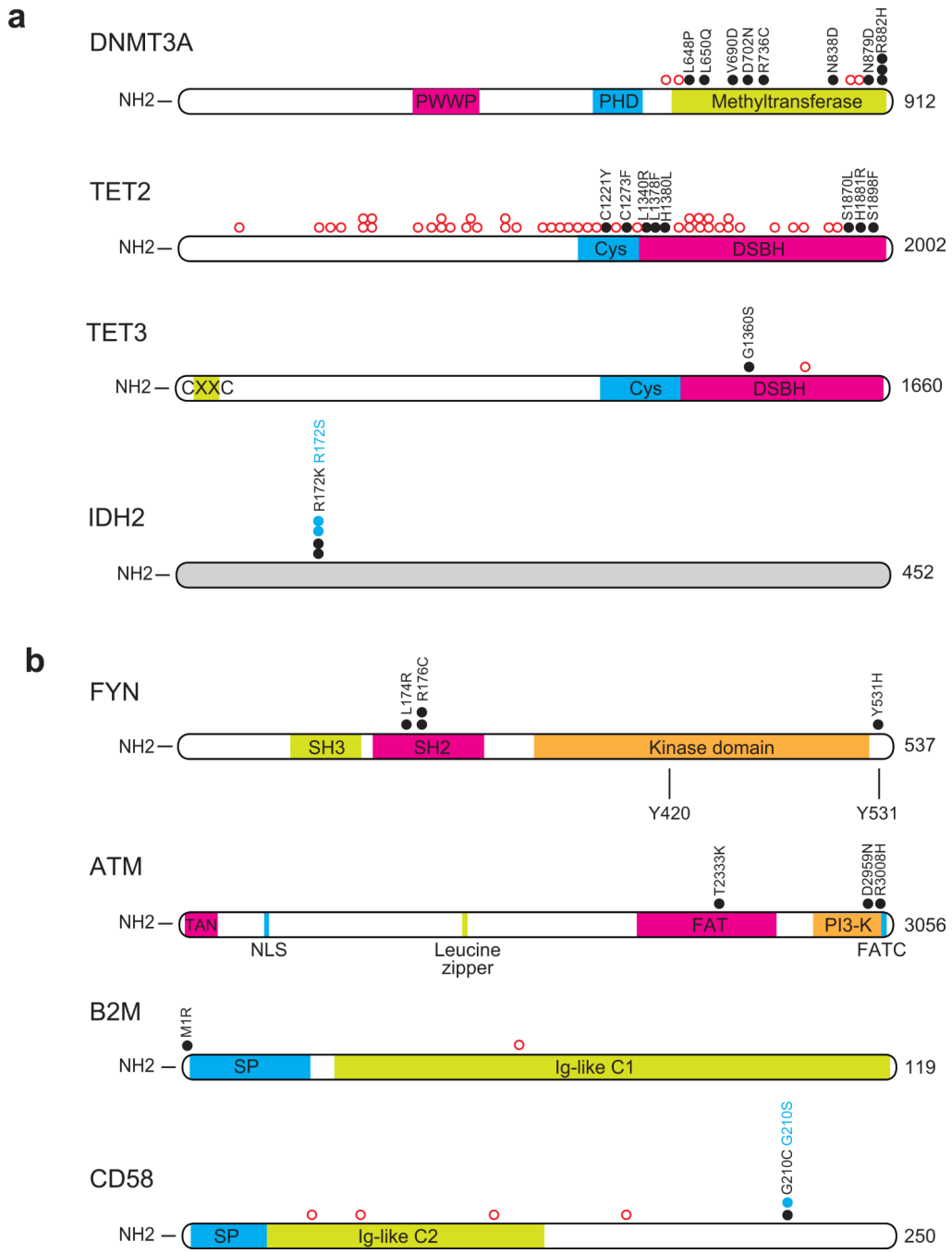

Figure 3. ***DNMT3A, TET2, IDH2, FYN, ATM, TET3, B2M*** **and** ***CD58*** **mutations in PTCLs**

a) Schematic representation of DNMT3A, TET2, TET3 and IDH2 proteins showing DNA methylation and hydroxymethylation related mutations in PTCL patients via exome sequencing (n=12) and amplicon resequencing (n=64). **b**) Schematic representation of FYN, ATM, B2M and CD58 protein variants identified in PTCL samples (n=12) and amplicon resequencing (n=64). Solid circles indicate predicted amino acid substitutions. The position of truncating mutations is indicated with red open circles. Multiple circles in the same amino acid position account for multiple patients with the same variant.

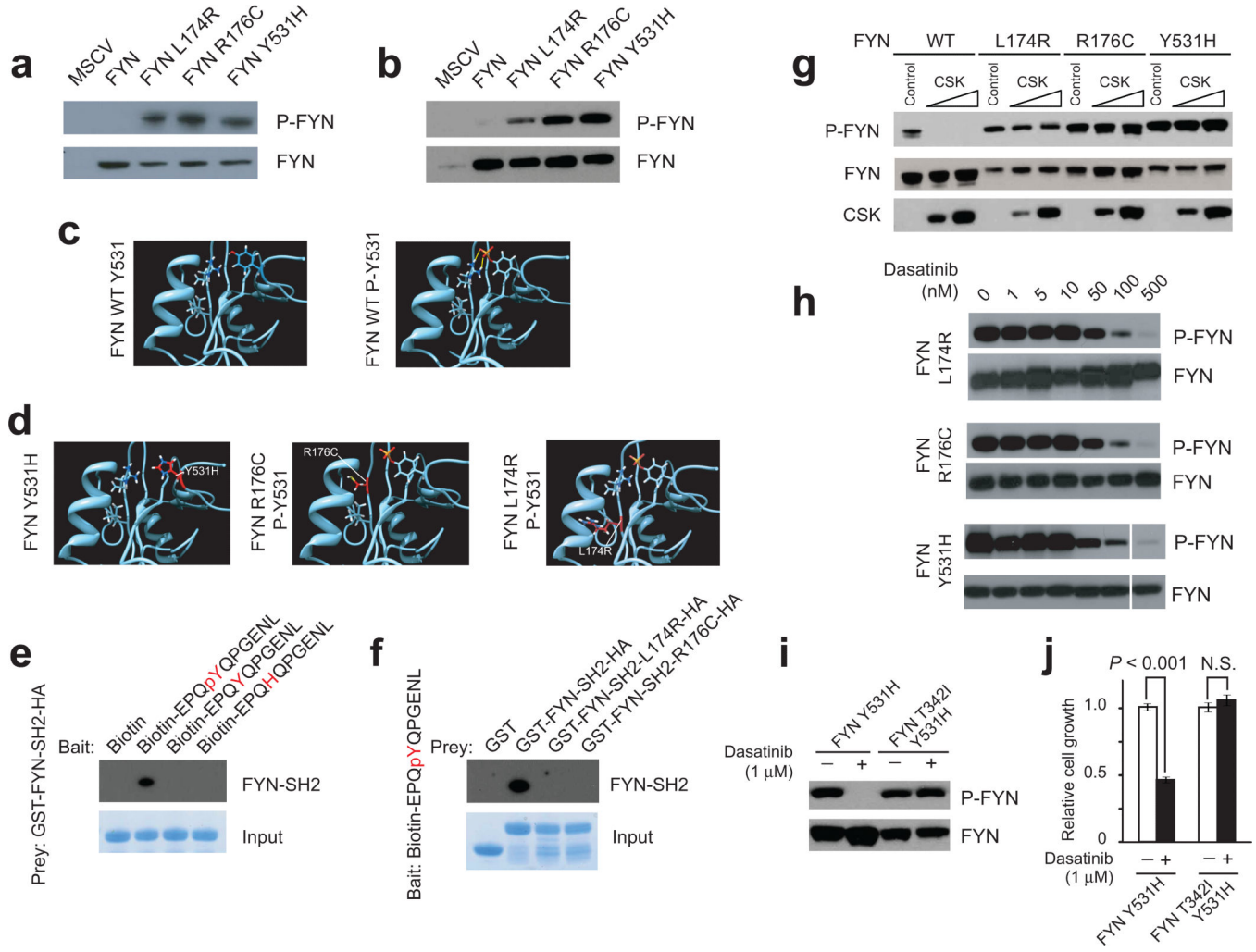

Figure 4. Structure modeling and functional characterization of *FYN* mutations identified in PTCLs

(**a**) Analysis of FYN activation via phospho-SRC immunoblotting in Rat1A cells infected wild type and PTCL associated FYN mutants expressing retroviruses. (**b**) Analysis of FYN activation via phosphor-SRC immunoblotting of FYN immunoprecipitates from Rat1A cells infected with wild type and PTCL associated FYN mutants expressing retroviruses. (**c**) Molecular ribbon representation of wild type FYN protein structure showing the positioning of the FYN SH2 domain and the C terminal Tyr531 phosphosite. (**d**) Structure modeling of FYN Tyr531His, FYN Arg176Cys and FYN Leu174arg mutant proteins. (**e**) Analysis of wild type GSTSH2-FYN interaction with C-terminal FYN peptides corresponding to wild type Tyr531 FYN, wild type P-Tyr531 FYN and mutant Tyr531His FYN via Western blot analysis of GST-SH2-FYN proteins in streptavidin-biotin C-terminal FYN peptide pull downs. Experiment was replicated twice. (**f**) Analysis of P-Tyr531 FYN C-terminal FYN peptide interaction with wild type GST-SH2-FYN and GST-SH2-FYN Leu174Arg and GST-SH2-FYN Arg176Cys mutant proteins via Western blot analysis of GST-SH2-FYN proteins in streptavidin-biotin P-Tyr531 C-terminal FYN peptide pull downs. (**g**) Western blot analysis of CSK inhibition of FYN activity in HeLa cells expressing wild type and

PTCL associated FYN mutant proteins. (**h**) Western blot analysis of dasatinib inhibition of FYN activity in HEK293T cells expressing PTCL associated FYN mutant proteins. (**i, j**) Analysis of dasatinib effects on FYN phosphorylation (**i**) and relative cell growth (**j**) in transformed Rat1A cells expressing the constitutively active FYN Tyr531His or the dasatinib-resistant FYN Thr342Ile Tyr531His double mutant protein. Data in (**j**) shows average ± s.d. from triplicate samples. *P* values were calculated using the two-tailed Student's *t* test.